Supercond. Sci. Technol. **23** (2010) 025013 (6pp) doi:10.1088/0953-2048/23/2/025013

Estimation of temperature rise from trapped field gradient on superconducting bulk magnetized by multi-pulse technique

Hiroyuki Fujishiro[1], Tomoyuki Naito[1], Kosuke Kakehata[1], Yosuke Yanagi[2] and Yoshitaka Itoh[2]

[1] Faculty of Engineering, Iwate University, 4-3-5 Ueda, Morioka 020-8551, Japan
[2] IMRA Material R&D Co. Ltd, 2-1 Asahi-cho, Kariya 448-0032, Japan

E-mail: fujishiro@iwate-u.ac.jp

Received 29 July 2009, in final form 6 October 2009
Published 18 December 2009
Online at stacks.iop.org/SUST/23/025013

Abstract
Trapped field profiles of the GdBaCuO superconducting bulk of 65 mm in diameter have been measured as magnetized using a successive pulsed-field application (SPA) and a subsequent iterative pulsed-field magnetization with reducing amplitude (IMRA). The trapped field gradient dB_T/dx on the bulk periphery increases concomitantly with increasing pulse number in the IMRA part. The dB_T/dx value on the bulk magnetized by field-cooled magnetization (FCM) was also measured at each temperature T_F. The maximum temperature T_{max} for each pulse was estimated by comparing the dB_T/dx value for the IMRA part with that for the FCM at each temperature. Furthermore, T_{max} was measured directly for the SPA part in the drilled hole in the bulk. The estimated T_{max} was nearly equal to the measured T_{max}, which thereby confirmed that T_{max} after applying the pulsed field can be estimated using the dB_T/dx value in the bulk periphery. The enhancement of the total trapped flux Φ_T^P in the IMRA part with increasing pulse number results from enhancement of the critical current density J_c because of the reduction in T_{max}.

1. Introduction

Practical applications using REBaCuO superconducting bulk (RE: rare earth ions and Y) as a strong quasi-permanent magnet have been intensively investigated for magnetic separation for environmental cleaning [1], drug delivery systems (DDSs) in medical applications [2] and sputtering cathodes to grow thin films for use in semiconductor devices [3]. Field-cooled magnetization (FCM) using a superconducting magnet is a conventional technique to magnetize bulk samples. The trapped field B_T^{FC} and the total trapped flux Φ_T^{FC} by FCM achieves the maximum abilities of the bulk. On the other hand, pulsed-field magnetization (PFM) has been studied intensively because it is compact, mobile and uses no superconducting magnet for practical applications. The trapped field B_T^P by PFM was, however, smaller than B_T^{FC} because of the large temperature rise due to the dynamical motion of the magnetic flux. To enhance B_T^P, it is necessary to decrease the temperature rise. Several approaches have been used such as a multi-pulse technique with stepwise cooling (MPSC) [4] and an iteratively pulsed-field magnetization with reducing amplitude (IMRA) [5]. We have studied the time and spatial dependences of the temperature, local field and trapped field on the surface of cryo-cooled REBaCuO bulk samples systematically during PFM for various starting temperatures T_s and applied fields B_{ex} [6, 7]. Considering the experimental results obtained, we have proposed a new PFM technique—designated as the modified multi-pulse technique with stepwise cooling (MMPSC)—and have produced the highest trapped field of 5.20 T at 29 K on a GdBaCuO bulk sample of 45 mm diameter, in which only 3.6 T had been trapped using a single-pulse application at 40 K [8].

Recently, REBaCuO superconducting bulks with diameter larger than 60 mm have been put onto the commercial market. Even a single-grain bulk of 140 mm diameter can be realized [9]. According to a Bean critical state model [10], a trapped field B_T at the bulk centre is proportional to the diameter of the bulk disc d. A total trapped flux density Φ_T is proportional to d^3, if the critical current density J_c of the bulk material is of equal value. The large Φ_T value is especially

Table 1. The trapped field B_T and total trapped fluxes Φ_T on the GdBaCuO bulk of 65 mm in diameter and 18 mm in thickness used in this study magnetized by the SPA, MMPSC and IMRA methods. Those on the GdBaCuO bulk of 45 mm in diameter and 18 mm in thickness are also shown. (Note: SPA: successive pulsed-field application. MMPSC: modified multi-pulse technique with stepwise cooling. IMRA: iteratively pulsed-field magnetization with reducing amplitude. FCM: field-cooled magnetization.)

	Method	⌀65 mm bulk [11, 13] (at 40 K)	⌀45 mm bulk [14] (at 30 K)
B_T^{FC} (T)	FCM	1.9 (77 K)	1.8 (77 K)
B_T^P (T)	SPA	1.3	1.9
B_T^P (T)	MMPSC	3.0	3.1
B_T^P (T)	SPA + IMRA	1.4	—
B_T^P (T)	MMPSC + IMRA	—	3.14
Φ_T^P (0.5 mm) (mWb)	SPA	2.9	1.96
Φ_T^P (0.5 mm) (mWb)	MMPSC	—	1.64
Φ_T^P (0.5 mm) (mWb)	SPA + IMRA	5.05	—
Φ_T^P (0.5 mm) (mWb)	MMPSC + IMRA	—	2.51
Φ_T^P (4 mm) (mWb)	SPA + IMRA	4.1	—
Φ_T^P (5 mm) (mWb)	MMPSC + IMRA	—	1.79
Φ_T^{FC} (4 mm) (mWb)	FCM	4.44 (48 K)	—

useful for applications such as electric motors/generators and sputtering cathodes.

We have investigated the trapped field characteristics on the ⌀65 mm GdBaCuO bulk by successive pulsed-field application (SPA) and the MMPSC method [11, 12]. Table 1 presents results of B_T and Φ_T on ⌀65 mm GdBaCuO bulk obtained using several magnetizing techniques. The results for ⌀45 mm GdBaCuO bulk are also shown for comparison. The maximum trapped field on the ⌀65 mm bulk was as low as B_T^P = 1.3 T by SPA and B_T^P = 3.0 T by MMPSC at 40 K, which was smaller than those on the ⌀45 mm bulk because of the lower J_c. However, the Φ_T^P value for a large bulk can be enhanced easily using the IMRA method; the Φ_T^P (0.5 mm) value, which was measured at $z = 0.5$ mm above the bulk surface, was as high as 5.05 mWb on the ⌀65 mm bulk at $T_s = 40$ K using the SPA + IMRA method, which was about 1.7 times larger than that obtained using the SPA method ($\Phi_T^P = 2.9$ mWb) [13]. It was 2.2 times larger than that on the ⌀45 mm bulk by the MMPSC + IMRA method ($\Phi_T^P = 2.51$ mWb) [14]. The Φ_T^P (4 mm) value (=4.1 mWb) at 40 K using the SPA + IMRA method was as high as the Φ_T^{FC} (4 mm) value (=4.44 mWb) obtained using FCM under $B_{ex} = 3$ T at 48 K [13].

The increase of the Φ_T^P value obtained using the IMRA part results from the reduction in temperature rise by reducing the amplitude of the magnetic pulse [6]. As a result, the effective J_c increases and the magnetic flux is additionally trapped in the bulk periphery. The gradient of the magnetic field, trapped in the bulk periphery, is expected to be closely related to the maximum temperature after the magnetic pulse application if Bean's model governs, even roughly, the magnetizing process during PFM. However, no experimental results have been reported in the relevant literature.

Table 2. The conditions from A to C in the SPA + IMRA method performed in this study.

Condition	Condition A	Condition B	Condition C
T_s	40 K	40 K	60 K
$B1$ $(=B2=B3)$	6.6 T	5.4 T	6.6 T
$B5$	6.1 T	4.9 T	6.0 T
$B7$	5.4 T	4.2 T	5.3 T
$B9$	4.9 T	3.5 T	4.8 T
$B11$	4.2 T	—	4.2 T
$B13$	3.5 T	—	3.4 T

As described in this paper, we measure the magnetic field gradient dB_T/dx on the ⌀65 mm GdBaCuO bulk using the SPA + IMRA method. We estimate the maximum temperature T_{max} using the magnetic field gradient with the IMRA part by comparing the dB_T/dx value with that using FCM. We examine the propriety of the estimation of T_{max} using the magnetic field gradient by comparison with the measured T_{max} in a small hole in the bulk.

2. Experimental details

A 18 mm thickness ⌀65 mm GdBaCuO superconducting bulk disc (Nippon Steel Corp.) was used for this study. The trapped field characteristics for various magnetizing techniques are presented in table 1. Figures 1(a) and (b) respectively show the experimental set-ups for the SPA + IMRA method and for the FCM method. In figure 1(a), the bulk was mounted on a soft iron yoke cylinder and was tightly anchored onto the cold stage of a Gifford–McMahon (GM) cycle helium refrigerator. The magnetizing solenoid coil, which generated a pulse field up to $B_{ex} = 6.7$ T with a rise time of 12 ms, was placed outside the vacuum chamber. Figure 1(c) presents the experimental sequence used for the SPA + IMRA method. Table 2 shows the conditions of the SPA + IMRA method used for this study. Three conditions A–C were performed with various temperatures and applied fields in the SPA part. The starting temperature T_s of the bulk was maintained at 40 or 60 K. Three magnetic pulses (nos. 1–3) with nearly identical amplitudes $B1$ $(=B2=B3)$ were applied sequentially after re-cooling to T_s. From the no. 4 pulse, the IMRA process was started; the applied pulsed fields B_n $(\leqslant B_{n-1})$ were iteratively reduced to 3.5 T in 0.3 T steps at constant T_s. Two-dimensional trapped field profiles of B_T^P (4 mm) and B_T^P (0.5 mm) were mapped at distances $z = 4$ or 0.5 mm above the bulk surface, stepwise with a pitch of 1 mm by scanning an axial-type Hall sensor (F W Bell, BHA 921) inside the vacuum chamber using an x–y stage controller. The temperature of the bulk was measured independently during SPA using a Teflon-coated chromel–constantan thermocouple (76 μm in diameter) in the hole of 1 mm in diameter and 10 mm in depth drilled in the periphery of the bulk. We confirmed the lack of degradation of superconductivity by drilling a small hole in the bulk.

For the FCM experiment as presented in figure 1(b), the bulk was similarly tightly anchored onto the cold stage of the refrigerator. The FCM was performed at various temperatures T_F from 38 to 85 K using a cryo-cooled superconducting magnet. During FCM, the static magnetic field of 3 T was

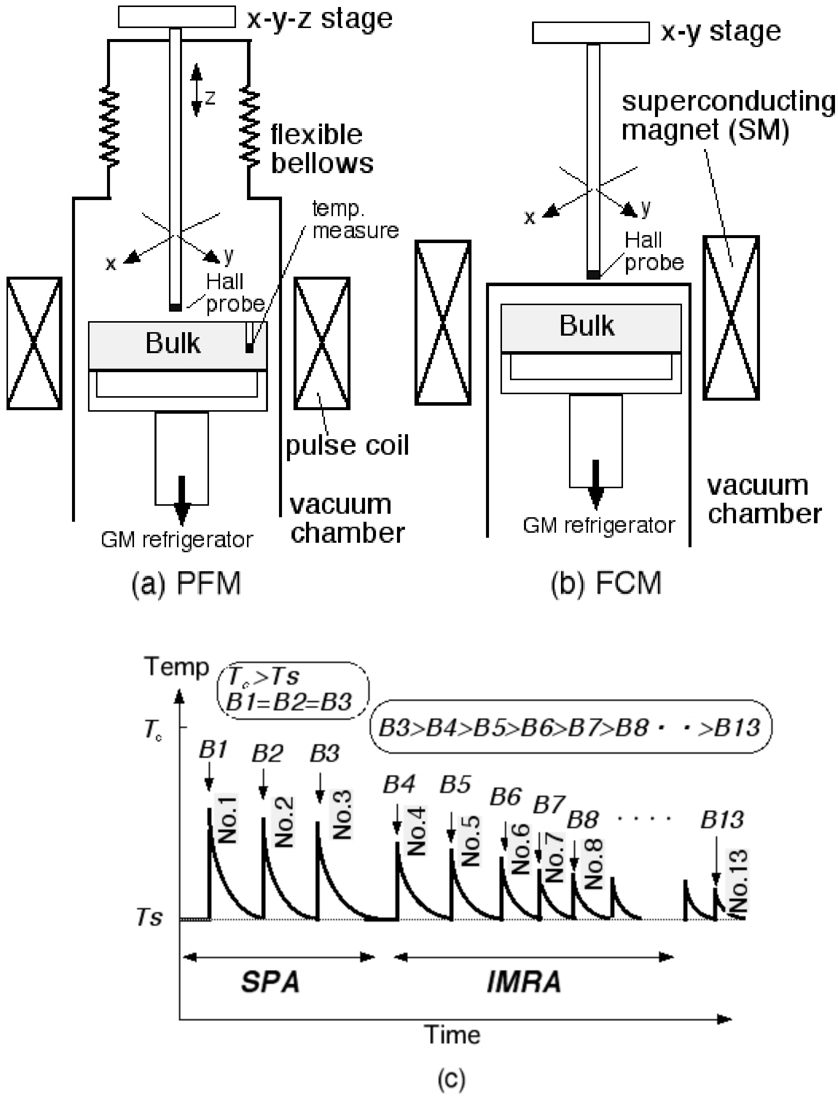

Figure 1. Experimental set-up around the bulk and magnetizing coil for (a) pulsed-field magnetization (PFM) and (b) field-cooled magnetization (FCM). For PFM and FCM, the trapped field profile was, respectively, measured inside and outside the vacuum chamber. (c) The experimental sequence of the SPA + IMRA method.

decreased to 0 T at 3 mT s^{-1}. B_T^{FC} (4 mm) profiles were measured on the vacuum sheath surface, which was 4 mm from the bulk surface.

3. Results and discussion

3.1. Trapped field distribution by FCM

Figure 2(a) shows a cross section of the trapped field profile B_T^{FC} (4 mm) by FCM at various temperatures T_F. For higher T_F, the cross section of the B_T^{FC} (4 mm) profile shows a cone shape, but the maximum B_T^{FC} (4 mm) value is low at the bulk centre. With decreasing T_F, the profile changed from conical to trapezoidal and the B_T^{FC} (4 mm) value increased and then saturated because of the increase of J_c with decreasing T_F. The FCM was performed under a constant magnetic field of 3 T. Therefore the saturation tendency took place. It is noteworthy that the magnetic field gradient increases concomitantly with decreasing T_F, as indicated by the dashed lines in the bulk periphery. According to Bean's model, the gradient of the trapped field is proportional to J_c [10]. Figure 2(b) presents the gradient of the trapped field $\mathrm{d}B_T^{FC}$ (4 mm)$/\mathrm{d}x$ as a function of temperature T_F. The gradient decreases with increasing T_F and then falls to zero at $T_c = 92$ K. Our group reported that the temperature on the bulk surface increased slightly during FCM and that the increase in temperature was enhanced with decreasing T_F and with increasing the descending speed of the magnetic field [15]. The descending speed in this study was 3 mT s^{-1}. Using the previous results, the respective temperature rise values were estimated as 4 K at $T_F = 50$ K, 2 K at 60 K and 1 K at 70 K, respectively.

3.2. Trapped field distribution by SPA + IMRA

Figures 3(a) and (b) respectively portray the pulse number dependence of the cross section of the trapped field profile

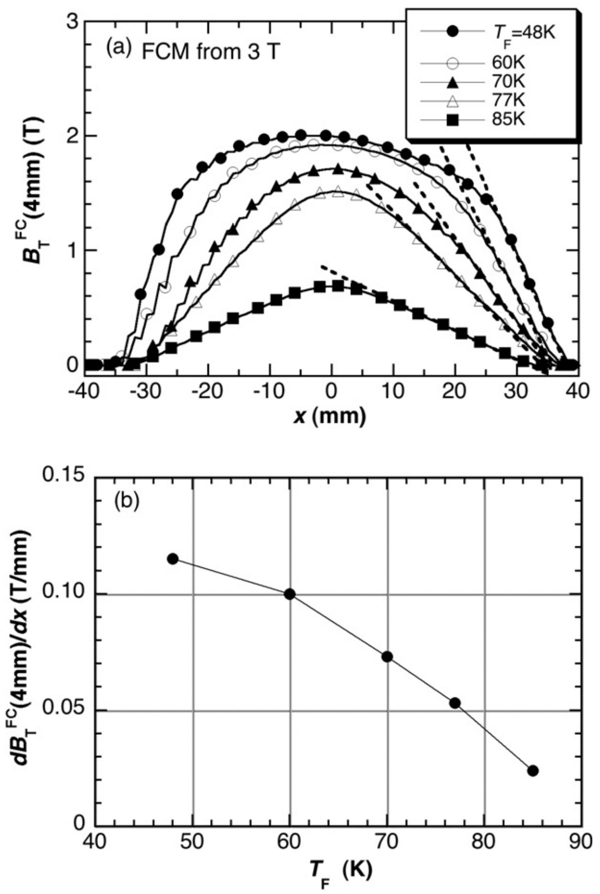

Figure 2. Trapped field profiles B_T^{FC} (4 mm) on the bulk for the FCM from 3 T for various temperatures T_F. (b) Magnetic field gradient dB_T^{FC} (4 mm)/dx as a function of temperature T_F.

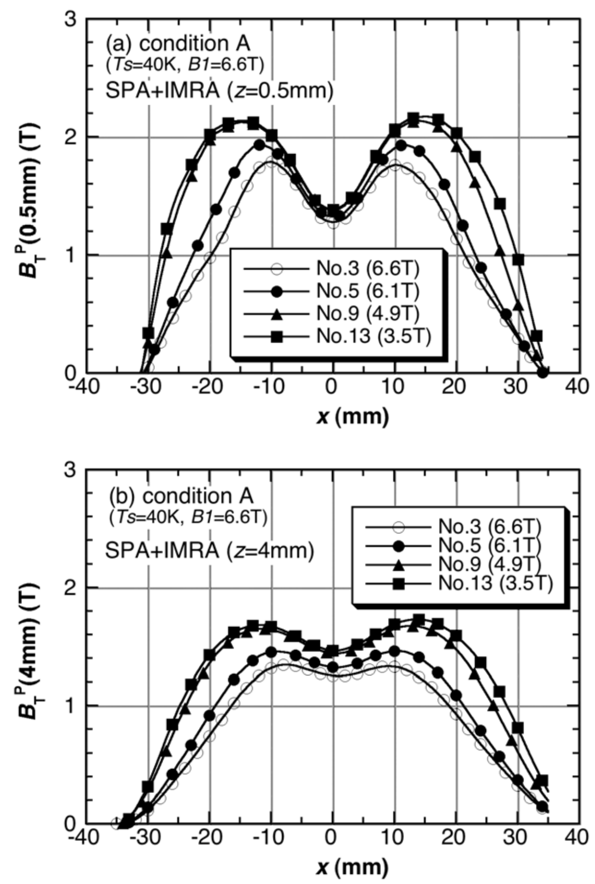

Figure 3. The pulse number dependence of the (a) B_T^P (0.5 mm) and (b) B_T^P (4 mm) profiles for the SPA + IMRA method of condition A ($T_s = 40$ K, $B1 = 6.6$ T).

B_T^P (0.5 mm) and B_T^P (4 mm) for 'condition A' ($T_s = 40$ K, $B1 = 6.6$ T) [13]. In figure 3(a), for the no. 3 pulse in the SPA part, the concave B_T^P (0.5 mm) profile is apparent. The B_T^P (0.5 mm) value at the bulk periphery increased gradually with increasing pulse number. On the other hand, the B_T^P (0.5 mm) value at the bulk centre increases only slightly. For the no. 13 pulse application ($B13 = 3.5$ T) in the IMRA part, the B_T^P increment at the bulk periphery seemed to saturate. In figure 3(b), the profile becomes broad and the magnitude of the B_T^P (4 mm) at the periphery becomes small because the measurement position is distant from the bulk surface. On the other hand, the magnitude of the B_T^P (4 mm) at the bulk centre was nearly the same as the B_T^P (0.5 mm) because of the concave B_T^P profile. The magnitude of the B_T^P at the bulk centre becomes small on increasing the distance z to larger than $z = 6$ mm. To compare the magnetic gradient by PFM with that by FCM and to estimate the temperature rise during the SPA + IMRA method, we adopted the B_T^P (4 mm) profiles for the following discussion, although the magnetic gradient should be measured just above the bulk surface. The B_T^{FC} (z) profile cannot be measured at $z = 0.5$ mm but at 4 mm because of the experimental limitation. The magnitude of the magnetic gradient for B_T^P (4 mm) was about 60% that for B_T^P (0.5 mm).

Figure 4(a) depicts the pulse number dependence of the cross section of the trapped field profile B_T^P (4 mm) for 'condition B' ($T_s = 40$ K, $B1 = 5.4$ T). The applied field $B1$ is smaller than that for condition A. Therefore, the magnetic flux cannot intrude into the bulk centre. For this reason, the trapped field profile becomes more concave. However, the magnetic gradient increased slightly with increasing pulse number in the IMRA part. Figure 4(b) depicts the pulse number dependence of the B_T^P (4 mm) profiles for 'condition C' ($T_s = 60$ K, $B1 = 6.6$ T). The operating temperature T_s is higher than that for condition A under an identical $B1$. Therefore, the magnetic flux can penetrate and be trapped at the bulk centre. The magnetic gradient increases concomitantly with increasing pulse number and the trapped field profile changes from conical to trapezoidal. It is noteworthy that the gradient of the trapped field at $T_s = 60$ K is smaller than that at $T_s = 40$ K.

Figure 5 presents the pulse number dependences of the magnetic gradient dB_T^P (4 mm)/dx for three conditions, which were determined from figures 3(b) and 4(a) and (b). The dB_T^P (4 mm)/dx value for condition B is larger than that for condition A because of the smaller temperature rise for lower applied field. The dB_T^P (4 mm)/dx value for condition A is greater than that for condition C because of the larger J_c at lower T_s. In all cases, the increase of the dB_T^P (4 mm)/dx value with increasing pulse number in the IMRA part arises from the reduction in the temperature rise. The dB_T^P (0.5 mm)/dx versus the pulse number n was also shown for condition A in

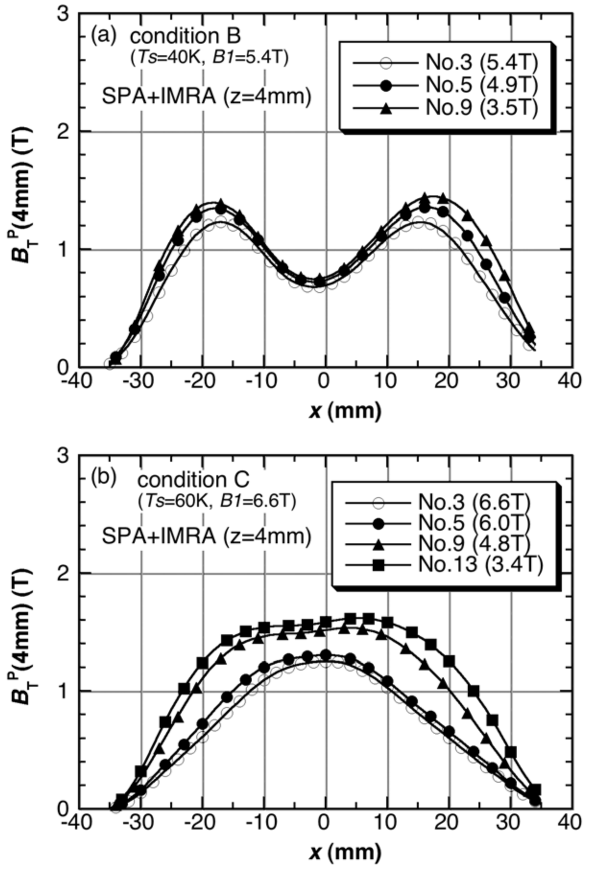

Figure 4. The pulse number dependence of the B_T^P (4 mm) profiles for the SPA + IMRA method of (a) condition B ($T_s = 40$ K, $B1 = 5.4$ T) and (b) condition C ($T_s = 60$ K, $B1 = 6.6$ T).

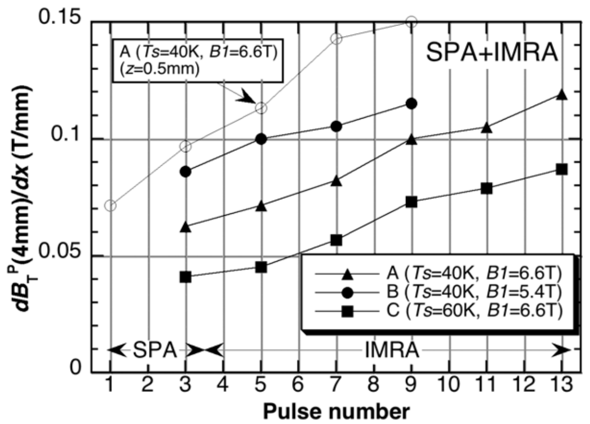

Figure 5. The pulse number dependence of the magnetic gradient dB_T^P (4 mm)/dx for conditions A, B and C, which were estimated from figures 3(b) and 4(a) and (b), respectively. The dB_T^P (0.5 mm)/dx versus the pulse number was also shown for condition A.

figure 5. The dB_T^P (0.5 mm)/dx is about 1.6 times larger than the dB_T^P (4 mm)/dx value and increases concomitantly with increasing pulse number.

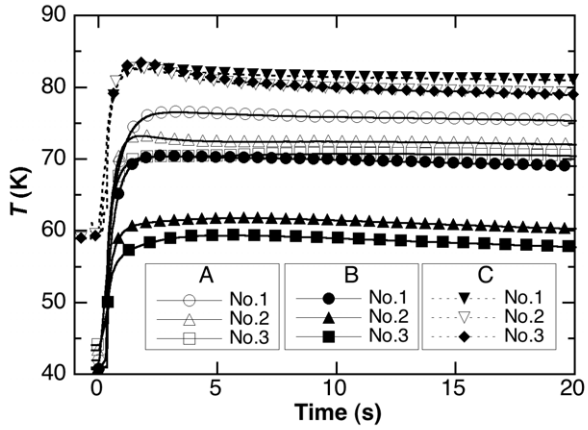

Figure 6. The time evolution of the temperature $T(t)$ in the bulk for the SPA part of conditions A–C.

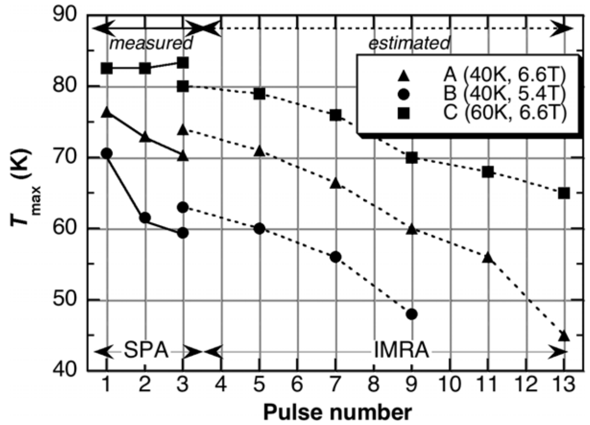

Figure 7. The pulse number dependence of the estimated T_{max} for each applied pulsed field ($n \geqslant 3$, dashed lines) and measured T_{max} ($1 \leqslant n \leqslant 3$, solid lines) for conditions A–C.

3.3. Measurement of temperature rise in the bulk

Figure 6 presents the time evolution of the temperature $T(t)$ in a small hole drilled in the bulk periphery for the SPA part of conditions A–C. The temperature rise for the no. 1 pulse is the largest and becomes small gradually for subsequent pulses. The maximum temperature T_{max} for the no. 1 pulse of condition A was 78 K; its temperature $T(t)$ was decreased gradually to 40 K for 15 min. T_{max} for condition C remains constant or increases slightly because of the powerful magnetic flux movement for each pulse.

3.4. Estimation of maximum temperature T_{max} during the SPA + IMRA method

We estimated the maximum temperature T_{max} for each step in the SPA + IMRA method using the results presented in figures 5 and 2(b). Figure 7 shows the pulse number dependence of the estimated T_{max}^E for $n \geqslant 3$ as dashed lines. The measured T_{max}^M values for $n \leqslant 3$, which are indicated in figure 6, are also shown as solid lines. The T_{max}^E decreased concomitantly with increasing pulse number for all conditions and approaches $T_s = 40$ K for conditions A and B and to

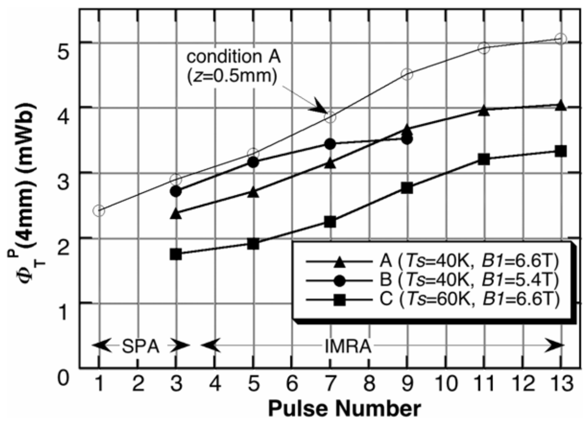

Figure 8. The pulse number dependence of the total trapped flux Φ_T^P (4 mm) for each condition. The Φ_T^P (0.5 mm) values for condition A are also shown.

$T_s = 60$ K for condition C. It is noteworthy that the measured and estimated T_{max} values for $n = 3$ are nearly equal, which suggests that the gradient of the trapped field profile is useful for estimation of T_{max}.

Figure 8 depicts the pulse number dependence of the total trapped flux Φ_T^P (4 mm) for each condition. The Φ_T^P (4 mm) value increases concomitantly with increasing pulse number; finally it saturates. It is noteworthy that the Φ_T^P (4 mm) values of condition B from $n = 3$–7 are larger than those of condition A. The estimated T_{max}^E of condition B is apparently lower. As a result, the J_c value is higher than with condition A. However, the maximum Φ_T^P (4 mm) value of 4.0 mWb was realized for the subsequent pulsed application of condition A, which was as high as Φ_T^{FC} (4 mm) by FCM under $B_{ex} = 3$ T at 48 K [13]. The Φ_T^P (0.5 mm) values for condition B are also shown in the figure, which are about 1.33 times larger than Φ_T^P (4 mm).

4. Summary

The trapped field profiles of the GdBaCuO superconducting bulk (65 mm in diameter) were measured. The bulk sample was magnetized using a successive pulsed-field application and the subsequent iterative pulsed-field magnetization method with reducing amplitude (SPA + IMRA) and a field-cooled magnetization (FCM). The maximum temperature T_{max} after heat generation for each pulse in the SPA + IMRA method was estimated through comparison of the magnetic field gradient in the bulk periphery with that after the FCM. Important experimental results and conclusions obtained in this study are summarized as follows.

(1) T_{max} after the pulsed-field magnetization can be estimated using the gradient of the trapped field dB_T/dx in the bulk periphery by comparison with the magnetic field gradient on the bulk periphery magnetized by FCM.
(2) The estimated T_{max} was nearly the same as the measured T_{max}, which was measured directly in the drilled hole in the bulk during the SPA part.
(3) In a bulk as large as 65 mm in diameter, the total trapped flux Φ_T^P is enhanced by the IMRA method because of the decrease in the temperature rise, which is effective for practical applications.

Acknowledgment

This work is supported in part by a Grant-in-Aid for Scientific Research from the Ministry of the Education, Culture, Sports, Science and Technology, Japan (no. 19560003).

References

[1] Hayashi H, Tsutsumi K, Saho N, Nishijima N and Asano K 2003 *Physica* C **392–396** 745
[2] Mishima F, Takeda S, Izumi Y and Nishijima S 2006 *IEEE Trans. Appl. Supercond.* **17** 2303
[3] Yanagi Y, Matsuda T, Hazama H, Yokouchi K, Yoshikawa M, Itoh Y, Oka T, Ikuta H and Mizutani U 2005 *Physica* C **426–431** 764
[4] Sander M, Sutter U, Koch R and Klaser M 2000 *Supercond. Sci. Technol.* **13** 841
[5] Yanagi Y, Itoh Y, Yoshikawa M, Oka T, Hosokawa T, Ishihara H, Ikuta H and Mizutani U 2000 *Advances in Superconductivity XII* (Tokyo: Springer) p 470
[6] Fujishiro H, Oka T, Yokoyama K and Noto K 2003 *Supercond. Sci. Technol.* **16** 809
[7] Fujishiro H, Yokoyama K, Oka T and Noto K 2004 *Supercond. Sci. Technol.* **17** 51
[8] Fujishiro H, Tateiwa T, Fujiwara A, Oka T and Hayashi H 2006 *Physica* C **445–448** 334
[9] Sakai N, Kita M, Nariki S, Muralidhar M, Inoue K, Hirabayashi I and Murakami M 2006 *Physica* C **445–448** 339
[10] Bean C P 1962 *J. Phys. Rev. Lett.* **8** 250
[11] Fujishiro H, Tateiwa T, Kakehata K, Hiyama T and Naito T 2008 *Physica* C **468** 1477
[12] Fujishiro H, Tateiwa T, Kakehata K, Hiyama T, Naito T and Yanagi Y 2007 *Supercond. Sci. Technol.* **20** 1009
[13] Fujishiro H, Kakehata K, Naito T, Yanagi Y and Itoh Y 2009 *Physica* C **469** 1250
[14] Fujishiro H, Hiyama T, Naito T, Yanagi Y and Itoh Y 2009 *Supercond. Sci. Technol.* **22** 095006
[15] Oka T, Yokoyama K, Fujishiro H, Kaneyama M and Noto K 2005 *Physica* C **426–431** 794